

Material considerations and locomotive capability in catalytic tubular microengines

Gaoshan Huang,^a Joseph Wang^b and Yongfeng Mei^{*a}

DOI: 10.1039/c2jm16813h

Driven by potential applications, such as cargo transportation (drug delivery) and biosensing, catalytic microengines have been shaped into tubular geometries with embedded catalytic and functional materials. The microengines harvest chemical energy from catalytic and biocatalytic reactions to realize autonomous locomotion at low Reynolds number, mimicking natural biomotors. The motion dynamics of these tubular microengines can be well-analyzed by a developed body-deformation model. The composition and morphology of the microengine play a key role in its overall performance and capabilities. This article highlights recent advances in the preparation of tubular microengines, related material considerations, and in their motion (speed and direction) control and functionalization towards a wide range of important practical nanoscale applications.

Introduction

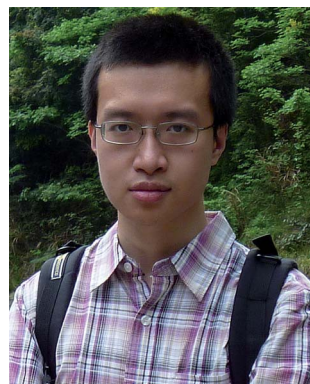
Controlled locomotion of micro-/nanoscale objects is of great importance since it is a fundamental step to realize micro-/nano-electro-mechanical systems which

may enable applications in electronics, photonics, bioengineering, drug delivery, nanomachinery, or nanoscale assembly.^{1,2} However, this may be challenging, mainly due to two factors. First, the Brownian motion becomes significant at such small scale, which may even dominate the movement of the object. Second, the influence originating from viscous force becomes large, especially in the fluid. This effect is quantitatively evaluated by the Reynolds number $Re = \rho v D / \eta$, where D is

the dimension of the object, and ρ and η are the density and viscosity of surrounding medium, respectively.³ For a micro/nano object in a fluid with a large viscosity, Re has a very small value, indicating that inertia plays an almost negligible role.³ The coasting time and the corresponding distance are extremely short and external forces must be exerted to maintain the locomotion.³ Conventional approaches to manipulate small objects require application of external

^aDepartment of Materials Science, Fudan University, Shanghai 200433, People's Republic of China. E-mail: yfm@fudan.edu.cn; Tel: +86-21-6564 3615

^bDepartment of Nanoengineering, University of California-San Diego, La Jolla, California, 92093, USA



Gaoshan Huang

Gaoshan Huang received his Ph.D. in condensed matter physics at the Nanjing University, China in 2007. After graduation, he worked in IFW Dresden, Germany as a guest scientist for two years. Then he moved to IMRE, Singapore as a research engineer. In 2010, he joined the Department of Materials Science, Fudan University, China, as an associate professor. His current research interest is the fabrications and characterizations of low-dimensional structures.



Joseph Wang

Joseph Wang received his Ph.D. from the Technion in Haifa in 1978. He held a Regents Professorship and a Manasse Chair positions at NMSU, and served as the director of Center for Bioelectronics and Biosensors of Arizona State University (ASU). He is currently a Professor in the Department of Nanoengineering at the University of California, San Diego (UCSD). His scientific interests are concentrated in the areas of nanobiotechnology, bioelectronics, nanomachines, and biosensors.

fields such as electric or magnetic fields,^{4–6} that are not capable to move the objects individually. Alternatively, optical tweezers are engaged to transport individual small objects using light intensity gradient, but this method needs special setup and is rather time-consuming.^{7,8} In fact, nature has built sophisticated biostructures through millions years of evolution to harness chemical energy from the environment for motion.^{9,10} For instance, kinesin obtains energy from hydrolysis of energy-rich adenosine triphosphate (ATP) molecules to induce conformational changes and directional motion on microtubules.¹¹ Research efforts have been devoted to produce hybrid microdevices utilizing protein-based biological motors. However, their limited lifetime *in vitro* and the narrow range of environmental conditions they can tolerate are also noticed.⁹ Thus, preparing artificial autonomous microengines, mimicking the mechanism of biomotors, is therefore of great interest since external fields are no longer needed and tasks can be performed by “smart” microengines *via* self-assembly. Several man-made microengines powered by catalytic reactions have so far been realized. These microengines are faster and stable although the structures are less complicated. Motivated by Whitesides’s early work where a plate is self-propelled by O₂ bubbles from Pt-catalytic decomposition of H₂O₂,¹² pioneering studies demonstrated that metallic heterostructures (*e.g.* bi-metal nanorods and sphere dimers) can serve as micro-/nano-engines in the presence of a H₂O₂ fuel.^{13–18} Preparation of other micro-/nano-engines from non-metal materials was also

reported.^{19,20} Despite substantial efforts aimed at understanding the mechanism of autonomous motion behaviors of those engines, controversies still exist among different deduced mechanisms based on independent experiments.^{9,13,14,18,21}

Compared to rod- or sphere-based micro-/nano-engines, recently introduced autonomous tubular microengines²² are considered to be the newest generation and offer distinct advantages. It is already well established that the motion mechanism of these tubular microengines involves a bubble-induced self-propulsion.^{22–24} Such microengines have already received an enormous attention owing to their fast motion speed (up to 3 mm s⁻¹)²⁵ and salt-independent motion behavior,²⁴ which cannot be observed in rod- or sphere-based micro-/nano-engines and thus hold considerable promise for important potential biomedical applications.²³ So far the tubular microengines were prepared *via* template-assisted electrosynthesis^{24,25} and rolled-up technology.^{22,26,27} The resulting micro-/nanotubular structure with diameter ranging from tens of nanometres to tens of micrometres are of benefit to design and manufacture autonomous microengines for future applications. As illustrated in Fig. 1(a), tubular microengines can be functionalized with bioreceptors for isolation of certain biomaterials.^{26,27} In addition, the design sketch in Fig. 1(b) schematically shows the structure of a conceptual “smart” microengine system, where the left part integrates a microengine and a battery, and the right part acts as an antenna as well as a microengine.²⁸ A steering unit manipulated by the controller can change the

movement of the system when the antenna receives a “command”. In addition, such “smart” systems can communicate with each other while performing complicated transportation tasks. For instance, the front end of the flat area is designed for a sensor and a drug delivery component (Fig. 1(b)). A microengine with dual microtubular structure (Fig. 1(c)) as the first step towards this “smart” system has already been reported.²⁹ Overall, the high propulsion power in biological media, precise direction control, and ease of surface functionalization of tubular microengines have made these microscale motors extremely attractive for a wide-range of applications.

In this highlight article, we discuss recent studies related to the catalytic tubular microengines that provide a deeper understanding regarding the materials selection, chemistry and motion mechanism of the self-propulsion at low Reynolds number. The controllability and potential applications of these catalytic tubular microengines will also be discussed.

Tubular geometries

Template-assisted synthesis.

Template-assisted electrosynthesis is quite common in micro-/nano-fabrications. Two different template electrodeposition protocols have so far been reported for preparing catalytic microengines.^{24,25} The first one is a conical Ag microwires onto which other metals can be easily electrodeposited to form coaxial structures.²⁴ Subsequent dissolution of the Ag wires leads to microtubular structures with inner diameters equal to the outer diameters of the Ag wires. The second recently reported template preparation route involves a commercial cyclopore polycarbonate membrane.²⁵ The template provides an attractive asymmetric structure by using one portion of the double cone (Fig. 2(a)), where aniline monomers are initially polymerized on the inner wall, leading to a rapid formation of a polyaniline (PANI) film. A Pt layer is subsequently plated inside the PANI tube using a galvanostatic method,²⁵ as show in the schematic diagram in Fig. 2(a). The conical PANI/Pt bi-layer microtube is ultimately obtained after the template dissolution. A



Yongfeng Mei

Yongfeng Mei received his Ph.D. at City University of Hong Kong in 2005. After that, he joined the Max Planck Institute for Solid State Research as a post-doctoral researcher. In 2007, he moved to IFW Dresden as a group leader in the Institute for Integrative Nano-sciences. In 2010, he joined Department of Materials Science, Fudan University, China as a full professor in materials chemistry and physics. His research interest focuses on the development of novel inorganic nanomembranes.

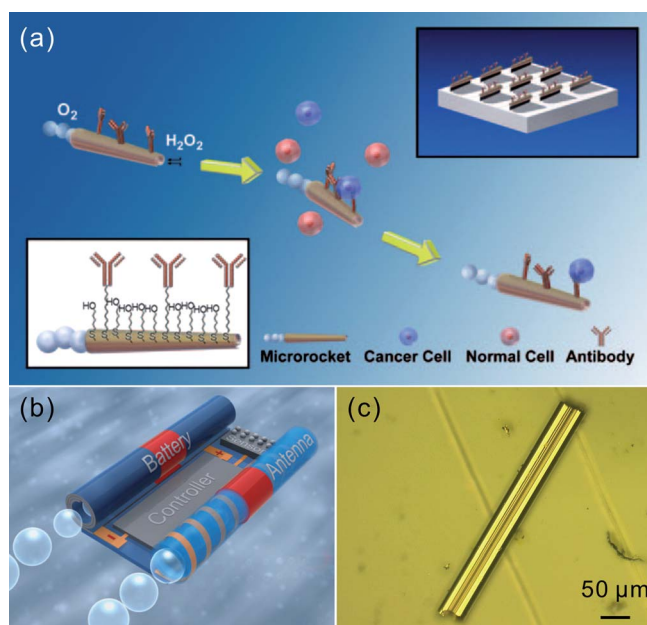


Fig. 1 (a) Microengines for selective loading and transportation of cancer cells. Upon encountering the cells, the microengines functionalized with anti-carcinoembryonic antigen (anti-CEA) monoclonal antibody (mAb) recognize the CEA surface antigens on the target cancer cells, allowing their selective loading and transportation. The top-right and bottom-left insets illustrate the structure of the as-modified microengines. Reproduced from ref. 26. (b) Proposed sketch for “smart” micro-engine system. The main components are two microtubular structures, where the left one integrates a microengine and a battery, and the right one acts as an antenna as well as a microengine. The controller is positioned in between. The front end of the flat area is occupied by a sensor and a drug delivery component. Adapted from ref. 28. (c) Dual microtubular structure which may work as dual microengine. Adapted from ref. 29.

typical microtube has a defined geometry with outer diameters of 2 and 1.1 μm , inner diameters of 1.5 and 0.5 μm , and a taper angle of 3.2°. The cross view of a PANI/Pt microtube is displayed in Fig. 2(b), which shows the thicknesses of PANI and Pt layers are 180 and 80 nm, respectively.

Self-rolled nanomembranes. The so-called rolled-up technology utilizes the intrinsic strain gradients inside the

nanomembranes to assemble three-dimensional micro-/nano-structures such as microtubes and microsprings.^{30,31} The strain gradient perpendicular to the surface is introduced by lattice mismatch in bi-layer semiconductor nanomembrane grown on a sacrificial layer by epitaxy.^{30–36} After selective etching of the sacrificial layer, the nanomembrane becomes free-standing and the strain gradient causes the bending/rolling of the nanomembrane. The approach was previously

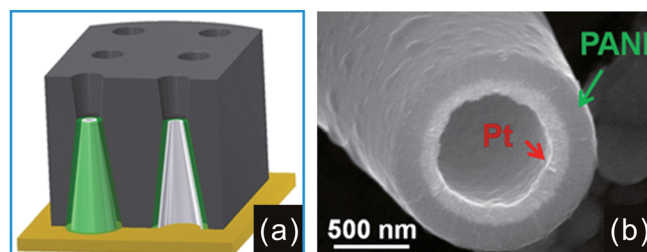


Fig. 2 (a) Template-assisted fabrication of tubular structure for microengine. Polyaniline (PANI) and Pt were electrodeposited sequentially into the commercial Cyclopore polycarbonate membrane. (b) Cross view of a PANI/Pt microtube. Adapted with permission from ref. 25. W. Gao, S. Satayamasithit, J. Orozco and J. Wang, *J. Am. Chem. Soc.*, 2011, **133**, 11862. Copyright 2011 American Chemical Society.

limited to semiconductor materials because the strain gradients are precisely controlled in epitaxial film. Although the controllability is not as perfect as those in epitaxy, the existence of a strain gradient was reported in other deposition methods due to inherent strain or the variation in thermal expansion.^{37,38} Taking these two factors into consideration, we recently developed a modified approach for making nanomembranes from a broad range of inorganic materials and their combinations rolling into microtubular structures.^{22,28} As outlined in Fig. 3(a),³⁹ a bi-/multi-layer nanomembrane is deposited on photoresist layer by the traditional approach *e.g.* sputtering or evaporation, and the microtube is fabricated upon removal of photoresist in organic solvent, which hardly attacks the inorganic nanomembrane.²² The opening of a typical microtube fabricated is exhibited in Fig. 3(b). It is worth noting that the photoresist layer serves not only as a sacrificial layer but also as a medium to transfer the designed patterns to the deposited nanomembrane since the photoresist layer itself can be easily patterned by photolithography,^{22,40} and the geometry of the microtube is tunable *via* pre-shaping nanomembrane before rolling. The important tube diameter, on the other hand, is mainly determined by the nanomembrane thickness and the strain gradient therein. The later is experimentally found to be introduced by changes in deposition rate, base pressure, and temperature.²²

Materials for locomotion and the dynamics

The catalytic tubular microengines are believed to be self-propelled by the recoiling force of accumulated gas bubbles.^{22,24,25,28,39} In most cases, catalytic microengines produce the required gaseous oxygen by a chemical decomposition reaction accelerated by a metallic catalyst: $2\text{H}_2\text{O}_2 \rightarrow 2\text{H}_2\text{O} + \text{O}_2$. The catalysts commonly, Ag²² or Pt,^{26,27,39} must be placed as the inner surfaces of the microtubular structures which act as chemical reaction chambers and storage cavities simultaneously. The typical metal structures reported in the literature are Pt/Au,²⁴ Pt/Ni/Au,²⁴ PANI/Pt, and PANI/Ni/Pt²⁵ for microtubular structures fabricated with the assistance of templates and

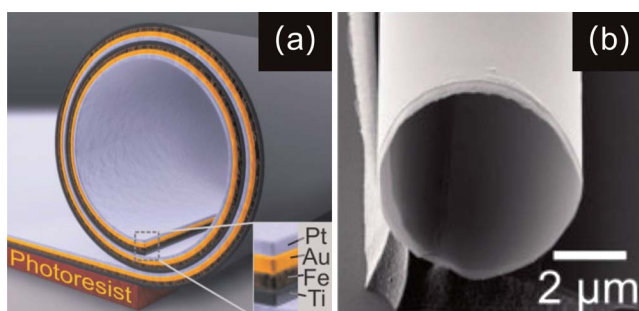


Fig. 3 Schematic diagram of a rolled-up tubular structure for microengine. The typical structure consists of Pt/Au/Fe/Ti multi-layer and self-rolled from a photoresist sacrificial layer. (b) SEM images of a rolled-up microtube. Adapted from ref. 39.

Pt/Au/Fe/Ti,³⁹ Ti/Fe/Au/Ag,²² Ti/Cr/Pt,⁴¹ Ti/Co/Pt,²⁹ and Ti/Ni/Au/Pt²⁷ for self-rolled nanomembranes. Magnetic layers may be incorporated to provide the possibility of remote magnetic control.^{28,39}

In principal, any well-controlled chemical reaction with or without catalysts involving a gaseous production can be engaged in such kind of self-propelled microengines working in corresponding liquid fuel. However, probably due to the simple chemical mechanism and the high efficiency of the catalytic decomposition of H₂O₂ by noble metals, the reaction is used in almost all the catalytic tubular microengines until recently when a biocatalytic microengine was demonstrated.⁴² In this microengine, a Au layer formed the inner surface of the tubular chamber by rolling a Ti/Au bi-layer nanomembrane and the Au layer is further functionalized by a self-assembled monolayer (SAM) of 3-mercaptopropionic acid (3-MPA). The carboxylic terminal groups of the SAMs were converted to amine-reactive esters by the coupling agents 1-ethyl-3-[3-dimethylaminopropyl] carbodiimide hydrochloride and N-hydroxylsuccinimide to covalently bind the protein (*i.e.* catalase) *via* carbodiimide reaction.⁴² As one of the most efficient enzymes, catalase has the ability to decompose millions of H₂O₂ molecules per second,^{42,43} and the efficiency is found to be even higher than that of the metallic catalyst. Experimental results exhibited that gas can be produced in H₂O₂ solution with very low concentration to propel the microengine. Microengines harvesting energy from other chemical reactions can be expected in the future.

When a catalytic tubular microengine is immersed into the fuel (*i.e.* H₂O₂ solution so far), the gas is produced at the nucleation site on the surface of the catalyst (noble metals or catalase) and then collected by the cavity forming microbubbles. The constraint of the channel make the microbubbles become gas slugs which cut the adjacent solution into liquid slugs. As we know, the geometries of microengines are conical channels due to the imperfection in the rolling process or by intended design.^{24–27,39} Thus, the different Laplace pressures between both menisci of such liquid slugs drag them to the end of tubular structure with a smaller diameter, while the gas slugs are moved along the opposite direction towards the larger opening.^{44,45} The microbubble is ultimately expelled, and thrusts the microengine forward one step.^{22,28,39} This process is the key to understanding the mechanism of the locomotion in one step at low Reynolds number. Previous investigation based on the experimental observation preliminarily disclosed that the average speed of microengine is approximately equal to the product of the bubble radius and expulsion frequency.³⁹ Based on this idea, the dynamics of the microengine are quantitatively described by a recently established body-deformation model.⁴⁶ In this model, the microengine and the microbubble are considered to be one system, as displayed in Fig. 4. The system experiencing a cyclic deformation from “microengine with a bubble inside” to “microengine with a detached bubble” in one step of autonomous motion in the cavity produces a gaseous bubble migrating along the channel axis to the

large opening (stage 1 in Fig. 4(a)),⁴⁷ and this does not generate driving force.⁴⁶ The microengine thrusts only when the gas bubbles starts to be expelled out of the cavity through the opening ($t = t_0$).^{39,46} After time point t_0 , the bubble is considered to move with a speed of $v_b(t)$ caused by the pressure in the cavity, and the recoiling force pushes the microengine to move in opposite direction with a increasing speed of $v_e(t)$ (stage 2 in Fig. 4(a)). The separating movements of both microengine and bubble continue until the moment of detachment (stage 3 in Fig. 4(a)). Observations demonstrate that after detachment the viscosity forces on the microengine (F_{engine}) and bubble (F_{bubble}) finally decrease $v_b(t)$ and $v_e(t)$ to zero respectively and the system evolves to stage 4 ($t = t_1$). A one step autonomous movement (from t_0 to t_1) is thus accomplished.⁴⁶ Calculation shows that the

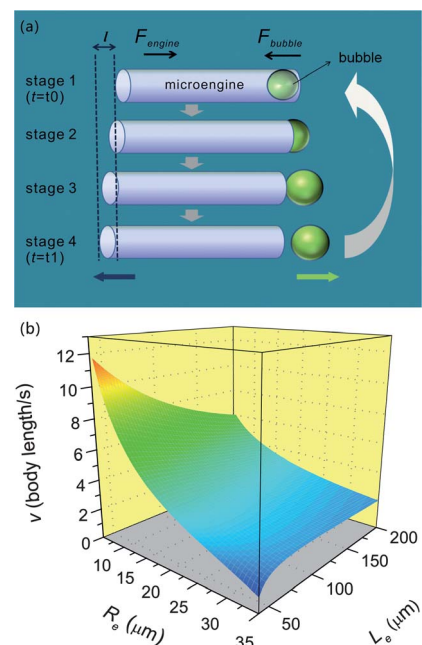


Fig. 4 (a) Schematic diagram of the body-deformation model, illuminating the locomotion in one step. The system makes a cyclic change from “microengine with a bubble inside” (stage 1) into “microengine with a detached bubble” (stage 4) which causes the motion of the microengine. The drag forces acting on the microengine and the bubble are F_{engine} and F_{bubble} respectively. (b) Calculated speed v in the form of body length/s as a function of R_e and L_e . Parameters used in the calculation: $n = 9.8 \times 10^{-4} \text{ m s}^{-1}$, $C_{\text{H}_2\text{O}_2} = 5\%$, and $R_b = R_e$. Adapted from ref. 46.

moving distance in one step l (see Fig. 4(a)) can be expressed as

$$l = \int_{t_0}^{t_1} v_e(t) dt$$

$$= \frac{6R_b^2}{3R_b + L_e / \left(\ln \left(\frac{2L_e}{R_e} \right) - 0.72 \right)} \quad (1)$$

where R_b is the bubble radius, L_e and R_e are the length and radius of the tubular cavity of microengine, respectively.⁴⁶ With the motion of the microengine, the fuel is pumped into the cavity from the front opening,³⁹ sustaining the chemical reaction. As long as the microengine is refilled, the moving process cycles to achieve continuous locomotion. The number of cycles accomplished in one second is determined by the gas produced and the volume of gas bubble, and therefore, in the case of the microengine driven by catalytic decomposition of H_2O_2 , the average speed of the microengine v is

$$v = \frac{9nC_{H_2O_2}R_eL_e}{3R_b^2 + L_eR_b / \left(\ln \left(\frac{2L_e}{R_e} \right) - 0.72 \right)} \quad (2)$$

where $C_{H_2O_2}$ is the H_2O_2 concentration and n is the O_2 production rate. Fig. 4(b) displays the calculated speed v in the form of body length/s as a function of R_e and L_e , indicating a significant influence of the microengine geometry on its dynamics. One should note that although this model is simple with some approximations, a close agreement between the experimental and calculated results is noted.⁴⁶

The above model considers the movement of the bubble along the axis of tubular cavity and only the longitudinal interaction is included, which therefore leads to a linear motion behavior of the microengine. However, the real situation could be complicated. For instance, due to the imperfection in the geometry, the cavity may be slightly curved and the opening may not be ideally circular. The expelling of the gas bubble thus deviates from the cavity axis, resulting in different movement behaviors, as reflected by the visualizing trajectories consisting of microbubble tails (see Fig. 5).^{25,39} In addition, during rapid production of gas, bubbles could be expelled from the front side of the microengine,⁴⁶ which may remarkably influence its motion status.^{42,46} The excitation of eddy flows at

high speed disturbing the linear motion of the microengine was also witnessed recently.⁴¹

Motion control of microengines

The engines in the real world should be controlled, and this requirement is also applicable to microengines performing tasks in the micro-/nano-world, *e.g.* in lab-on-a-chip applications.¹⁰ Several approaches have been developed for regulating the speed and controlling the direction of the catalytic tubular microengines.

Speed control. For a certain microengine, the motion speed is actually determined by the gas production. Hence, it is natural to assume the speed is connected to the fuel concentration,²⁵ which is proved by the above model if the gas production rate in catalytic decomposition is a constant (see eqn (2)). However, a linear dependence cannot always be observed due to the limitation in catalyst surface area or intrinsic turnover rate at high fuel concentration, and a speed maximum can only be reached at an optimal fuel concentration.^{28,47} In the microengine with an inner Pt surface, the hydrophobic nature of Pt refrains from intimate contact with the aqueous fuel solution. Introduction of surfactant effectively reduces the surface tension of the liquid and leads to a better wetting of the Pt surface. This promotes the gas production rate and consequently accelerates the microengine.^{24,25,47} With increasing surfactant concentration, the surface tension becomes constant,⁴⁸ and the formed surfactant aggregates may occupy the active sites of the catalyst surface, leading to a decrease of speed.⁴⁷ Furthermore, it is well known that the gas production rate is accelerated at higher temperatures. This temperature dependence has been exploited towards a dramatic acceleration of catalytic tubular microengine (up to 200 body lengths/s) even in a very low fuel concentration by heating the fuel solution to physiological temperature, relevant to bioapplications.⁴¹ In reverse, by cooling the fuel solution, the microengines can be completely brought to a halt at ~ 2 °C.⁴¹ In fact, low temperature is not the only way to shut off the microengine. It was reported recently that light illumination

can be engaged to control the microengine movement around a Pt layer.⁴⁹ The illumination of the H_2O_2 solution with light in the presence of a Pt layer diminishes the concentration of fuel and degrades the surfactant in the vicinity, reducing the reaction rate in the nearby microengine, and in turn contributes to the turning off of the microengine. The effect becomes remarkable if the distance between the microengine and Pt layer is small or the light wavelength is short.⁴⁹

Direction control. Magnetic guidance represents a common and convenient way to control the directionality of self-propelled microengines.^{24–27,39,47,50,51} This involves the incorporation of a magnetic layer (*e.g.* Ni, Fe, or Co) into the tube wall and application of an external magnetic field.^{24–27,39,47,50,51} Optical microscopy on a working catalytic tubular microengine with a magnetic layer clearly demonstrated that it can be turned or rotated, suggesting the microengine is remotely controllable.^{24,26,27,39,51} If the magnetic field is rotating with a constant frequency f , the microengine previously moving in straight line with speed of v will be localized in circular trajectory with radius $r = v/(2\pi f)$, which means the localization radius decreases with increasing the rotating frequency.³⁹ A more accurate control has recently been achieved by a combination of magnetic field manipulation and microfluidic channel confinement.^{27,52} The microengine in the microchannel exhibits a similar locomotion behavior to those in free bulk solution, and the energy harvested from the chemical reaction is high enough to support a self-propelling against the flowing stream in the microchannel.⁵²

Self-assembly at the interface. The catalytic tubular microengines normally swim in the fuel liquid. However, if the density of the fuel is increased on purpose by mixing with a medium of high density,⁵³ the increased buoyancy force may lift the microengine to the surface of the liquid, and therefore the air/liquid interface can significantly influence the motion behavior of the microengine.⁵³ Micro-objects such as bubbles produced by the microengine itself or a glass capillary create curved interfaces which can attract the microengine due to the meniscus-climbing effect, as in the

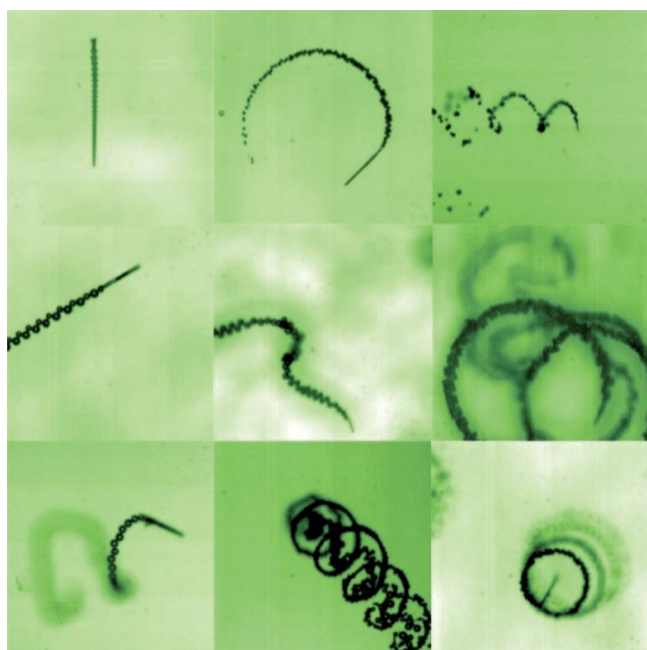


Fig. 5 Trajectories of microbubble tails for different motions. Adapted from ref. 39.

coating with a thin Au layer, the microengine is functionalized with anti-carcinoembryonic antigen (anti-CEA) monoclonal antibody (mAb). The motion of the functionalized microengine in serum with dilute H_2O_2 can selectively bind to target cancer cells (Fig. 1(a)) and then effectively transport them in serum to destination with the help of magnetic field as shown in Fig. 6(b).²⁶ Similar approaches involving microengines functionalized with different bioreceptors, such as oligonucleotides, aptamers or lectins, have been used recently to enable rapid and selective transportation or isolation of nucleic acid, protein, and bacterial targets, respectively.^{23,27,51,55}

Conclusions and outlook

This highlight article has summarized recent advances involving catalytic tubular microengines which harvest energy from chemical reactions. The catalytic material as the inner surface of the microtubular cavity accelerates the gas production by fuel decomposition and the recoiling force of accumulated gas bubbles expelling out of the cavity propels the microengine. The dynamics of the locomotion at low Reynolds number is found to be determined by the recoiling force and drag force which are connected with the surrounding chemical environment and the geometry of the microengine. The motion speed and direction of a microengine can be well controlled by external efforts to fulfil complex tasks. Overall, the composition and morphology of the microengine thus play a key role in its overall performance and capabilities.

Future developments in the field lie in several aspects. First, the fabrication technologies can be improved to fabricate complicated three-dimensional structures in a controllable way, because the geometry of the microengine significantly influences the dynamics. The uniformity of the structures will also be very important for parallel mass production. Second, new catalysts or new (*e.g.*, hierarchical) catalytic structures—used in energy conversion—should be explored for high efficiency. Although the catalytic decomposition of H_2O_2 can be highly efficient, reliance on H_2O_2 fuel should be avoided in practical biological applications (particularly *in vivo*). Therefore, microengines engaging other catalysts or chemical reactions for efficient gas

behavior of water striders.^{29,53,54} The balance between the capillary and recoiling forces further determines assembly and disassembly of the microengines. An experiment was carried out to demonstrate this dynamic self-assembly process. Once the glass capillary is immersed into the liquid fuel, microengines run towards the capillary and attach to it. When the capillary is removed from the liquid, microengines move away randomly. One may infer that the motion of the microengine can be manipulated by introducing artificial air/liquid interfaces.

Potential applications

The high propulsion power and large towing forces displayed by tubular microengines in unprocessed biological fluids hold considerable promise for diverse practical applications. So far, the catalytic tubular microengines demonstrate very good ability in cargo transportation.^{24,47} Experiments showed that the cargo can be loaded by physical means, for example, magnetic force.²⁴ In addition, since the liquid is pumped into the front opening when the microengine is working,³⁹ cargos located close enough to the opening will be adsorbed and move with the microengine.⁴⁷ The moving direction of the microengine can be controlled by a magnetic field to realize multi-loading of polystyrene microparticles, as demonstrated in Fig. 6(a).

When the microengine and the cargos are directed by the magnetic field to the destination, cargo delivery is performed by a rapid rotation of the magnetic field.⁴⁷ During the transportation, the attachment between the cargo and the microengine is also physical without any selectivity, so different objects such as non-magnetic metallic plates⁴⁷ and cells⁵⁰ can be transported. To achieve complex tasks in biology, loading with selectivity is required. Researchers have successfully functionalized the outer surface of the microengine for selective bonding of biomaterials.^{26,27,51,55} As displayed in the insets of Fig. 1(a), after

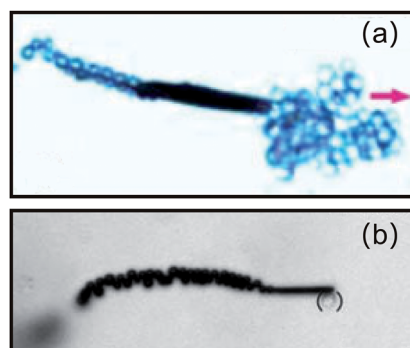


Fig. 6 (a) Optical microscopy images of microengine loading and transporting 44 polystyrene microparticles. Adapted from ref. 47. (b) Optical microscopy images of an anti-CEA mAb-modified microengine transporting a CEA+ pancreatic cancer cell in serum. Adapted from ref. 26.

production are of practical importance. Third, modifying microengines with more functions to perform transportation and isolation tasks is very promising. It is anticipated that transportation of different targets or multiplexed detection will come into reality by using microengines functionalized with different bioreceptors, which may ultimately result in numerous practical applications like biomedical diagnostics and environmental monitoring, etc. Finally, intelligent microengines could be developed. The self-assembly process of the microengines indicates the task can be accomplished by a group of microengines as a collective behavior rather than by an individual microengine. As demonstrated in Fig. 1(b), the conceptual "smart" microengine system may have the communication unit so that they can collaborate with each other to accomplish challenging tasks.²⁸

Acknowledgements

This work is supported by the Natural Science Foundation of China (Nos. 61008029 and 51102049), Program for New Century Excellent Talents in University (No. NCET-10-0345), and "Shu Guang" project by Shanghai Municipal Education Commission and Shanghai Education Development Foundation. J.W. was supported by the U.S. Natural Science Foundation (Award Number CBET 0853375).

References

- 1 Y. P. He, J. S. Wu and Y. P. Zhao, *Nano Lett.*, 2007, **7**, 1369.
- 2 W. F. Paxton, S. Sundararajan, T. E. Mallouk and A. Sen, *Angew. Chem., Int. Ed.*, 2006, **45**, 5420.
- 3 E. M. Purcell, *Am. J. Phys.*, 1977, **45**, 3.
- 4 Marcel Dekker, *Interfacial Electrokinesics and Electrophoresis* (Ed.: Á. V. Delgado), New York, USA, 2002.
- 5 H. Watarai, M. Suwa and Y. Iiguni, *Anal. Bioanal. Chem.*, 2004, **378**, 1693.
- 6 L. Zhang, J. J. Abbott, L. X. Dong, K. E. Peyer, B. E. Kratochvil, H. X. Zhang, C. Bergeles and B. J. Nelson, *Nano Lett.*, 2009, **9**, 3663.
- 7 S. M. Block, *Nature*, 1992, **360**, 493.
- 8 R. Agarwal, K. Ladavac, Y. Roichman, G. Yu, C. M. Lieber and D. G. Grier, *Opt. Express*, 2005, **13**, 8906.
- 9 J. Wang, *ACS Nano*, 2009, **3**, 4.
- 10 J. Wang and K. M. Manesh, *Small*, 2010, **6**, 338.
- 11 R. D. Vale and R. A. Milligan, *Science*, 2000, **288**, 88.
- 12 R. F. Ismagilov, A. Schwartz, N. Bowden and G. M. Whitesides, *Angew. Chem., Int. Ed.*, 2002, **41**, 652.
- 13 W. F. Paxton, S. Sundararajan, T. E. Mallouk and A. Sen, *Angew. Chem., Int. Ed.*, 2006, **45**, 5420.
- 14 T. Mirkovic, N. S. Zacharia, G. D. Scholes and G. A. Ozin, *Small*, 2010, **6**, 159.
- 15 L. F. Valadares, Y.-G. Tao, N. S. Zacharia, V. Kitaev, F. Galembeck, R. Kapral and G. A. Ozin, *Small*, 2010, **6**, 565.
- 16 D. Kagan, R. Laocharoensuk, M. Zimmerman, C. Clawson, S. Balasubramanian, D. Kang, D. Bishop, S. Sattayasamitsathit, L. F. Zhang and J. Wang, *Small*, 2010, **6**, 2741.
- 17 J. Wu, S. Balasubramanian, D. Kagan, K. M. Manesh, S. Campuzano and J. Wang, *Nat. Commun.*, 2010, **1**, 36.
- 18 J. G. Gibbs and Y.-P. Zhao, *Appl. Phys. Lett.*, 2009, **94**, 163104.
- 19 Y.-G. Tao and R. Kapral, *ChemPhysChem*, 2009, **10**, 770.
- 20 W. R. Browne and B. L. Feringa, *Nat. Nanotechnol.*, 2006, **1**, 25.
- 21 G. Rückner and R. Kapral, *Phys. Rev. Lett.*, 2007, **98**, 150603.
- 22 Y. F. Mei, G. S. Huang, A. A. Solovev, E. Bermúdez Ureña, I. Moench, F. Ding, T. Reindl, R. K. Y. Fu, P. K. Chu and O. G. Schmidt, *Adv. Mater.*, 2008, **20**, 4085.
- 23 S. Campuzano, D. Kagan, J. Orozco and J. Wang, *Analyst*, 2011, **136**, 4621.
- 24 K. M. Manesh, M. Cardona, R. Yuan, M. Clark, D. Kagan, S. Balasubramanian and J. Wang, *ACS Nano*, 2010, **4**, 1799.
- 25 W. Gao, S. Sattayasamitsathit, J. Orozco and J. Wang, *J. Am. Chem. Soc.*, 2011, **133**, 11862.
- 26 S. Balasubramanian, D. Kagan, C. J. Hu, S. Campuzano, M. Jesus Lobo-Castañon, N. Lim, D. Y. Kang, M. Zimmerman, L. F. Zhang and J. Wang, *Angew. Chem., Int. Ed.*, 2011, **50**, 4161.
- 27 D. Kagan, S. Campuzano, S. Balasubramanian, F. Kuralay, G.-U. Flechsig and J. Wang, *Nano Lett.*, 2011, **11**, 2083.
- 28 Y. F. Mei, A. A. Solovev, S. Sanchez and O. G. Schmidt, *Chem. Soc. Rev.*, 2011, **40**, 2109, and references therein.
- 29 J. X. Li, B. R. Lu, Z. K. Shen, Z. C. Xu, H. Li, J. J. Wen, Z. D. Li, X. P. Qu, Y. F. Chen, Y. F. Mei and R. Liu, *Microelectron. Eng.*, 2011, **88**, 1792.
- 30 V. Ya. Prinz, V. A. Seleznev, A. K. Gutakovskiy, A. V. Chehovskiy, V. V. Preobrazhenskii, M. A. Putyato and T. A. Gavrilova, *Phys. E*, 2000, **6**, 828.
- 31 O. G. Schmidt and K. Eberl, *Nature*, 2001, **410**, 168.
- 32 M. H. Huang, C. Boone, M. Roberts, D. E. Savage, M. G. Lagally, N. Shaji, H. Qin, R. H. Blick, J. A. Nairn and F. Liu, *Adv. Mater.*, 2005, **17**, 2860.
- 33 S. V. Golod, V. Ya. Prinz, V. I. Mashanov and A. K. Gutakovskiy, *Semicond. Sci. Technol.*, 2001, **16**, 181.
- 34 D. J. Thurmer, Ch. Deneke, Y. F. Mei and O. G. Schmidt, *Appl. Phys. Lett.*, 2006, **89**, 223507.
- 35 P. O. Vaccaro, K. Kubota and T. Aida, *Appl. Phys. Lett.*, 2001, **78**, 2852.
- 36 J. Q. Hu, Y. Bando, J. H. Zhan, M. Y. Liao, D. Golberg, X. L. Yuan and T. Sekiguchi, *Appl. Phys. Lett.*, 2005, **87**, 113107.
- 37 S. V. Golod, V. Ya. Prinz, P. Wägli, L. Zhang, O. Kirfel, E. Deckhardt, F. Glaus, C. David and D. Grützmacher, *Appl. Phys. Lett.*, 2004, **84**, 1.
- 38 M. H. Huang, F. Cavallo, F. Liu and M. G. Lagally, *Nanoscale*, 2011, **3**, 96, and references therein.
- 39 A. A. Solovev, Y. F. Mei, E. Bermúdez Ureña, G. S. Huang and O. G. Schmidt, *Small*, 2009, **5**, 1688.
- 40 G. S. Huang, Y. F. Mei, D. J. Thurmer, E. Coric and O. G. Schmidt, *Lab Chip*, 2009, **9**, 263.
- 41 S. Sanchez, A. N. Ananth, V. M. Fomin, M. Viehrig and O. G. Schmidt, *J. Am. Chem. Soc.*, 2011, **133**, 14860.
- 42 S. Sanchez, A. A. Solovev, Y. F. Mei and O. G. Schmidt, *J. Am. Chem. Soc.*, 2010, **132**, 13144.
- 43 L. Betancor, A. Hidalgo, G. Fernández-Lorente, C. Mateo, R. Fernández-Lafuente and J. M. Guisan, *Biotechnol. Prog.*, 2003, **19**, 763.
- 44 J. Bico and D. Quere, *J. Fluid Mech.*, 2002, **467**, 101.
- 45 J. C. T. Eijkel and A. V. D. Berg, *Lab Chip*, 2005, **5**, 1202.
- 46 J. X. Li, G. S. Huang, M. M. Ye, M. L. Li, R. Liu and Y. F. Mei, *Nanoscale*, 2011, **3**, 5083.
- 47 A. A. Solovev, S. Sanchez, M. Pumera, Y. F. Mei and O. G. Schmidt, *Adv. Funct. Mater.*, 2010, **20**, 2430.
- 48 H.-J. Butt, K. Graf and M. Kappl, *Physics and Chemistry of Interfaces*, Weinheim, Germany, 2003.
- 49 A. A. Solovev, E. J. Smith, C. C. Bof Bufon, S. Sanchez and O. G. Schmidt, *Angew. Chem., Int. Ed.*, 2011, **50**, 10875.
- 50 S. Sanchez, A. A. Solovev, S. Schulze and O. G. Schmidt, *Chem. Commun.*, 2011, **47**, 698.
- 51 J. Orozco, S. Campuzano, D. Kagan, M. Zhou, W. Gao and J. Wang, *Anal. Chem.*, 2011, **83**, 7962.
- 52 S. Sanchez, A. A. Solovev, S. M. Harazim and O. G. Schmidt, *J. Am. Chem. Soc.*, 2011, **133**, 701.
- 53 A. A. Solovev, Y. F. Mei and O. G. Schmidt, *Adv. Mater.*, 2010, **22**, 4340.
- 54 D. L. Hu and J. W. M. Bush, *Nature*, 2005, **437**, 733.
- 55 S. Campuzano, J. Orozco, D. Kagan, M. Guix, W. Gao, S. Sattayasamitsathit, J. C. Claussen, A. Merkoçi and J. Wang, *Nano Lett.*, 2012, **12**, 396.